ADVANCED MATERIALS INTERFACES
www.advmatinterfaces.de

Catalytic Performance of Pd Nanoparticles Obtained by Direct Reduction in Cellulose–Poly(ferrocenylsilane) Hybrid Sponges

Huan Cheng, Mark A. Hempenius, Xiaofeng Sui, and G. Julius Vancso**

Cellulose–poly(ferrocenylsilane) (PFS) polyionic liquid (PIL) composite sponges are fabricated by codissolution of cellulose and PFS-PIL, followed by solvent exchange and freeze-drying. The hybrid sponges are used to in situ produce and immobilize palladium nanoparticles (Pd NPs), leading to Pd NP-decorated porous supports. The formation of Pd NPs is confirmed by TEM and XPS measurements. The as-prepared cellulose/PFS-PIL@Pd sponges exhibit a high catalytic activity in the reduction of 4-nitrophenol (4-NiP) to 4-aminophenol (4-AmP). As a variety of metal NPs may be immobilized using this method, these sponges constitute a promising new class of catalytic porous supports.

1. Introduction

Metal nanoparticles (NPs) with unique characteristics such as nanoscale dimensions and high activity are widely used in catalytic applications.[1] However, metal NPs are often unstable due to their high surface energy. This leads to aggregation, limiting their applications at the nanoscale, as well as their catalytic performance.[2] Besides, the separation of metal NPs from the reaction medium is a challenge, and unrecycled metal NPs could cause environmental pollution.[3] Therefore, loading metal NPs onto a matrix is recognized as an effective method to improve their stability, processability, and reusability and to decrease the negative impact on the environment.[4]

Numerous studies have been devoted to developing matrices to immobilize metal NPs, such as metal-organic frameworks, microspheres, fibers, films, aerogels, and sponges.[1b,5] Among them, aerogels, or sponges, have received broad attention because they are easily separated and recovered from the reaction media.[6] Focusing on the choice of the materials for preparing aerogels, bio-based polymers (e.g., cellulose) are more appealing than the synthetic polymers due to their inherent "green" properties such as biodegradability, biocompatibility, and availability of abundant reserves, as well as low price.[7] Conforming cellulose and metal NPs into porous structures can in principle improve the immobilization and catalytic properties of metal NPs. Importantly, metal NPs can be easily recovered from catalytic reactions when these systems are employed, and the diffusion of reactants through the porous matrix can be enhanced.[8] Recently, cellulose aerogels and sponges have been used as supports for metal NPs. For example, bacterial cellulose aerogels were used as the matrix for supporting Cu and Ni NPs and applied in case studies of nitrophenol reduction.[9] In another example, gold NPs were supported on cellulose aerogel as an efficient catalyst for epoxidation of styrene.[10]

Commonly, the synthesis of metal NPs on the support requires toxic external reducing agents, such as N_2H_4 and KBH_4, with potentially harmful effects for the environment.[6a,11] Although cellulose with abundant hydroxyl groups can be used as both reducing agent and stabilizing environment for the synthesis of metal NPs, some additional harsh conditions such as long reaction time, high pressure, and temperature are usually needed if cellulose is employed as the sole reducing agent.[12] Therefore, developing a green and simple method to fix a reducing agent into the cellulose sponge matrix, which can reduce and immobilize metal NPs without being released into the environment to cause secondary pollution, is environmentally compelling. For example, in situ reduction of Pd NPs on the surface of cellulose nanofibers was achieved in the presence of polydopamine (PDA). The catechol moiety in PDA could reduce metal ions without adding any external reducing agent.[8a] Thiolated nanocellulose sponge was prepared from hydrolytic silane condensation of cellulose nanofibers and used as support to immobilize copper cations via in situ Cu^{II} to Cu^{I} reduction and complexation.[8c]

Poly(ferrocenylsilanes) (PFS), which consist of alternating ferrocene and silane units in the main chain, are a promising class of polymers that can be reversibly oxidized and reduced by chemical and electrochemical ways.[13] By postfunctionalization of PFS using different substituents, a range of organometallic polymers was received, including PFS-based hydrophilic polyionic

H. Cheng, X. Sui, G. J. Vancso
Key Lab of Science and Technology of Eco-Textile
Ministry of Education
College of Chemistry
Chemical Engineering and Biotechnology
Donghua University
Shanghai 201620, China
E-mail: suixf@dhu.edu.cn; g.j.vancso@utwente.nl
H. Cheng, M. A. Hempenius, G. J. Vancso
Sustainable Polymer Chemistry and Materials Science and Technology of Polymers
MESA+ Institute of Nanotechnology
University of Twente
P.O. Box 217, Enschede AE 7500, The Netherlands
The ORCID identification number(s) for the author(s) of this article can be found under https://doi.org/10.1002/admi.202101664.

DOI: 10.1002/admi.202101664

liquids,[14] and hydrophobic polyionic liquids[15] (PFS-PIL). Our group reported on a metal NP "foundry" based on a platform consisting of redox-active PFS hydrogels.[16] The concept of using a redox-active hydrogel for fabricating noble metal NPs, where the PFS network chains provide confinement and are employed as redox agents, i.e., no external reducing agents or ligands are required, is demonstrated to provide an effective platform.[17]

Herein, we propose an environmentally benign approach to decorating porous cellulose sponges with metal NPs using PFS-PIL as a fixed reducing agent, which also provides scaffolds for immobilization of NPs. PFS modified with imidazolium groups and ion-exchanged with hydrophobic counterions (dialysis in counterions solution) readily dissolves in ionic liquids and forms homogeneous solutions with cellulose. After solvent exchange and freeze-drying, the as-prepared composite sponges were thoroughly characterized by FTIR, SEM, TEM, XPS, and TGA. To exemplify their catalytic properties, the metal NP loaded sponges were applied for the reduction of 4-nitrophenol (4-NiP). The results obtained in this study demonstrate that the composite sponges are suitable supports for the generation, immobilization, and use of noble metal NPs in catalytic applications.

2. Results and Discussion

2.1. Fabrication of Cellulose/PFS-PIL@Pd Sponge

The chemical structures of PFS-PIL, cellulose, and ionic liquid used in this study are shown in **Figure 1**a. PFS-PIL is a cationic polyelectrolyte composed of a PFS main chain and butylimidazolium bis(trisfluoromethylsulfonyl)-imide side groups (PFS-C_4IM Tf_2N). The counterion in the PIL was exchanged to the Tf_2N^- to make it insoluble in water but soluble in DMF and ionic liquids, following the procedure developed by the Yuan group.[18]

Figure 1b illustrates the fabrication procedure leading to the composite sponge. To satisfy the requirements of an ecofriendly metal NPs support, we designed this composite sponge following three considerations: 1) the composite materials should be assembled into a 3D framework with a well interconnected open porous structure to guarantee the passage of reactant solution; 2) the sponge must be hydrophilic to ensure contact with reactants; 3) metal NPs should be uniformly dispersed and fixed on the pore walls to efficiently catalyze the reaction.

In this work, the ionic liquid (1-butyl-3-methylimidazolium chloride) was used as a solvent to dissolve cellulose. Ionic liquids have been used to replace regular organic solvents in a range of applications due to specific advantages such as excellent dissolution ability and ease of recycling.[19] Polar interactions between hydroxyl groups in cellulose and the anions and cations in ionic liquids favor dissolution. Hydrogen bonding interactions between hydroxyl groups in cellulose and both anions and cations in ionic liquids have been monitored by NMR spectroscopy.[20] The chemical structure of the butylimidazolium groups of PFS-PIL is similar to that of the ionic liquid used in the experiments. Hence, it can be expected that PFS-PIL dissolves in the ionic liquid employed. Indeed, a uniform and homogeneous solution of PFS-PIL and cellulose was

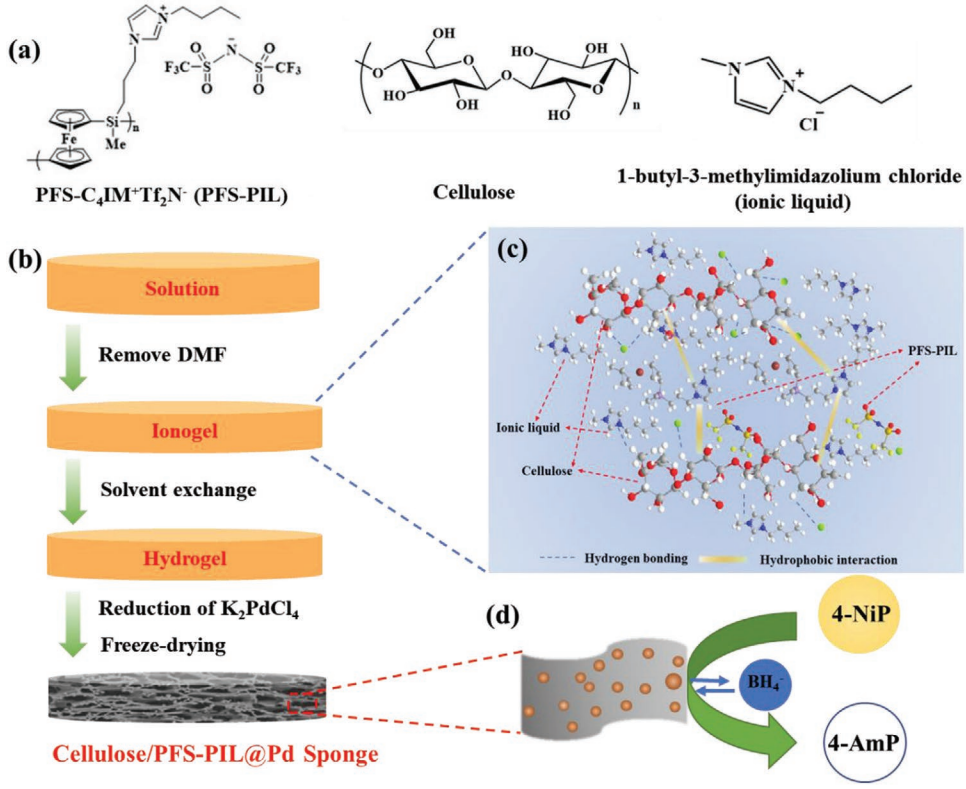

Figure 1. Preparation and application of the cellulose/PFS-PIL@Pd sponge. a) Chemical structure of PFS-PIL, cellulose, and ionic liquid used in this study. b) Schematic representation illustrating the preparation process of cellulose/PFS-PIL@Pd sponges. c) Schematic illustration showing the interactions among the components. d) Reduction of 4-NiP by the Pd NPs on the pore wall.

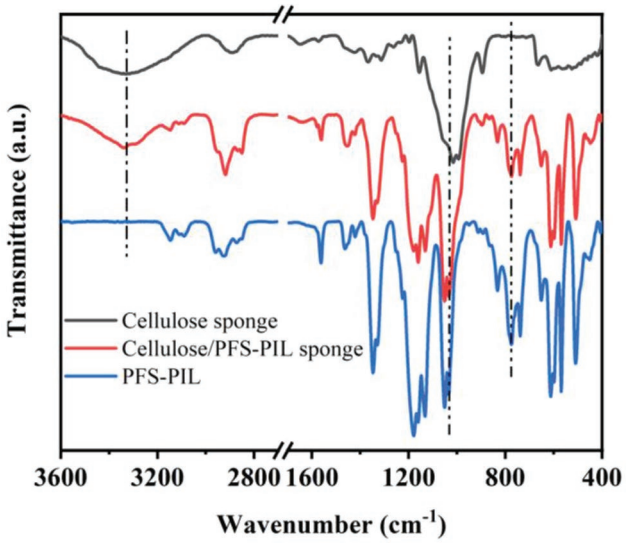

Figure 2. FTIR spectra of cellulose sponge, PFS-PIL, and cellulose/PFS-PIL sponge.

obtained (Figure 1c). After removal of the ionic liquid by solvent exchange and drying, a homogeneously colored PFS-cellulose composite resulted. It therefore seems reasonable to assume that hydrophobic interactions between the hydrophobic PFS main chains and parts of the ionic liquid side groups and cellulose, combined with polar interactions between the ionic liquid side groups of PFS-PIL and the hydroxyl moieties of cellulose, cause the observed uniform distribution of PFS-PIL over the cellulose support.

Functionalization of cellulose/PFS-PIL sponges with Pd NPs was achieved using two different approaches. In the first approach, cellulose/PFS-PIL hydrogels were placed in a 0.1×10^{-3} M K_2PdCl_4 solution. The PFS chains of the hydrogel reduced this salt to Pd NPs, which caused the hydrogel to turn brown. The porous structure obtained after freeze-drying of the hydrogel was denoted as cellulose/PFS-PIL@Pd sponge.

In a second approach, cellulose/PFS-PIL hydrogels were first freeze-dried and the resulting dry sponge was immersed in 0.1×10^{-3} M K_2PdCl_4 solution. In this process, the sponge was wetted but it retained its solid-like porous structure. Similar to the hydrogel case, the wetted sponge acquired a brown color as Pd NPs were formed. This porous structure was denoted as cellulose/PFS-PIL@Pd2 sponge. The catalytic performance of these two different sponges is investigated in the subsequent sections.

Unlike external reducing agents, the hydrophobic PFS-PIL remains in the hydrogel. Also, PFS-PIL contributes to the in-situ immobilization of metal NPs. Figure 1d shows the reduction mechanism of 4-nitrophenol to 4-aminophenol by Pd NPs, which is used to demonstrate catalytic activity as discussed later.

2.2. FTIR of Sponges

Cellulose sponge, PFS-PIL, and cellulose/PFS-PIL sponge were characterized by FTIR, the results are shown in **Figure 2**.

In the spectrum of cellulose sponge, a strong peak of the stretching vibrations of O—H groups around 3347 cm^{-1} characteristics for cellulose can clearly be seen. Characteristic peaks for PFS around 1037 and 774 cm^{-1} are also clearly present in the spectrum of PFS-PIL. After mixing them in ionic liquid and regenerating in water and freeze-drying, the FTIR spectrum of cellulose/PFS-PIL sponge contains both the characteristics of PFS (1037 and 774 cm^{-1}) and cellulose (3347 cm^{-1}), indicating a successful mixing of cellulose and PFS-PIL.

2.3. Morphology of Sponges

The morphologies of cellulose, cellulose/PFS-PIL, and cellulose/PFS-PIL@Pd sponges, respectively, were characterized by SEM and the results are shown in **Figure 3**.

All of these three sponges have a porous structure with large pores, and the porous structure did not change after adding PFS-PIL or after the reduction to obtain Pd NPs. With the growth of ice crystals during the freeze-drying process, the gel network composed of cellulose and PFS-PIL gradually arranged itself along the growing crystals, forming the porous structure observed in the SEM images.[21]

The pore size of these sponges is around 200 µm, which will allow reactants to pass through smoothly with stirring. In addition, the microporous structure not only provides channels but also provides a large area of contact between solutions and NP catalysts in the sponge, which contributes to the catalytic efficiency of these porous structures. The BET specific surface area was 5.24 $m^2\ g^{-1}$ and the Barrett-Joyner-Halenda (BJH) pore size distribution results indicated that there are nanoscale pores in the microporous wall (Figure S2, Supporting Information).

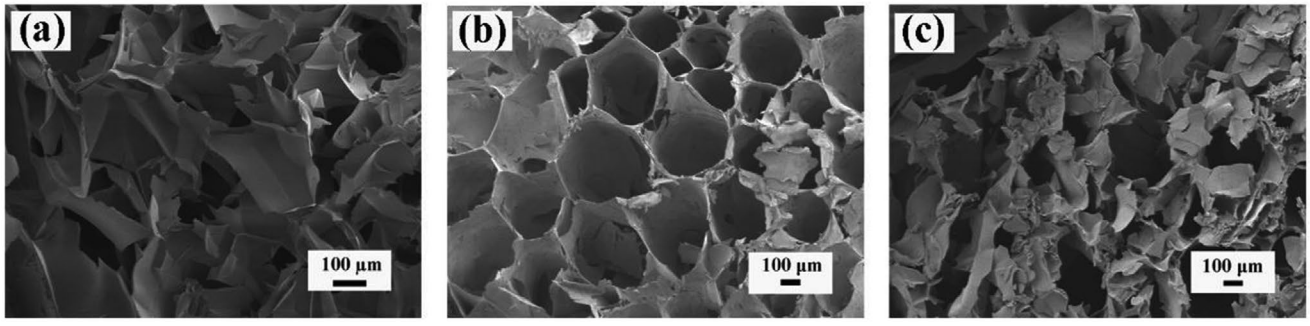

Figure 3. Morphology of the sponges. a) Cellulose sponge. b) Cellulose/PFS-PIL sponge. c) Cellulose/PFS-PIL@Pd sponge.

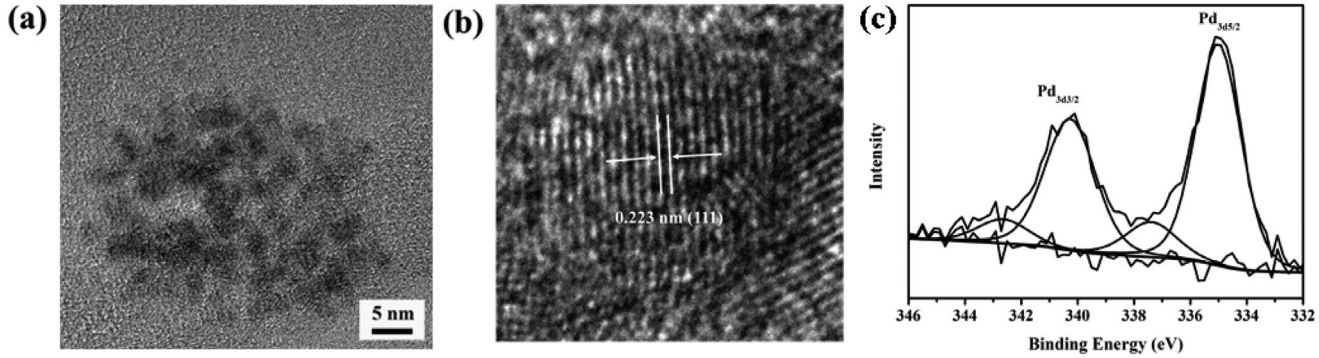

Figure 4. Characterization of Pd NPs. a) TEM image of Pd NPs. b) HR-TEM image of Pd NPs with many (111) facets exhibiting a spacing of lattice fringes of 0.223 nm. c) XPS spectrum of the Pd $_{3d}$ region of a cellulose/PFS-PIL@Pd sponge.

2.4. Characterization of Pd NPs

In order to verify the presence of Pd NPs, the cellulose/PFS-PIL@Pd hydrogel was imaged by TEM.

A representative TEM image of NPs formed in-situ is shown in **Figure 4**a. The diameter of Pd NPs was mainly in the range of 3–7 nm (Figure S3c, Supporting Information). A high-resolution TEM image of Pd NPs is shown in Figure 4b. The image clearly captures that these NPs include single crystals with several[111] facets exposed.[22] The measured interplanar spacing for the lattice fringes is 0.23 nm, corresponding to metallic Pd[111].[23]

The XPS spectrum shows double peaks with binding energies of 335.1 and 340.5 eV, corresponding to Pd $_{3d5/2}$ and Pd $_{3d3/2}$, respectively (Figure 4c), which are in good agreement with the standard values for Pd(0).[24] Combined with the results obtained by TEM, we can confirm that the Pd NPs were successfully obtained.

2.5. Thermal Gravimetry Analysis (TGA)

In the next section, we present thermal characterization data to demonstrate the thermal stability and decomposition features of the sponges discussed.

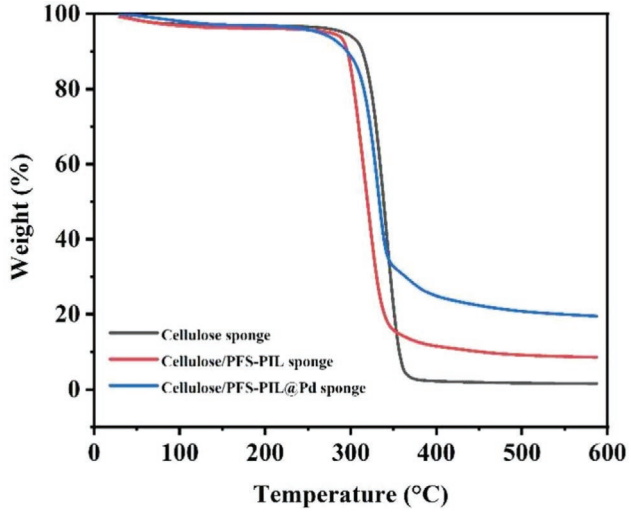

Figure 5. TGA results of cellulose sponge, cellulose/PFS-PIL sponge, and cellulose/PFS-PIL@Pd sponge.

Thermal gravimetry analysis (TGA) of a cellulose sponge, a cellulose/PFS-PIL sponge and a cellulose/PFS-PIL@Pd sponge was performed in a N_2 atmosphere. The results obtained are shown in **Figure 5**. For the cellulose sponge, substantial weight loss was found with an onset at around 300 °C, and the residual mass approached 2.0%, which is attributed to remaining carbon. For cellulose/PFS-PIL sponge, the residual mass approached 8.8%. This increased residual mass is ascribed to the formation of preceramic Fe—Si oxide (carbide) materials due to the presence of PFS.[25] After the reduction of K_2PdCl_4 to Pd NPs, the residual mass approached 19.5% due to the presence of Pd in the residue. The Pd content calculated from the residual mass is about 12.3%. The ICP-MS measurement was also used to quantify the Pd content in the sponge, resulting in a Pd content of almost 10%.

2.6. Catalytic Performance of Cellulose/PFS-PIL@Pd Sponges

The reduction of 4-NiP to 4-AmP (**Figure 6**a) is usually recognized as a model reaction to study the catalytic performance of metal NPs.[26] 4-NiP reduction obeys the classic Langmuir-Hinshelwood mechanism.[27] The BH_4^- ions in the system react with Pd metal particles at their surface and transfer hydrogen to the surface of these particles. Along with the generation of surface-bound hydrogen species, 4-NiP adsorbs onto unoccupied sites of the metal surface. Finally, in a rate-determining step, adsorbed 4-NiP is reduced to 4-AmP which subsequently desorbs.[27a] The absorbance peak of 4-NiP shifts from 320 to 400 nm as it is turned into a 4-nitrophenolate anion by the hydride ion originating from $NaBH_4$.[28]

Due to the excess of $NaBH_4$ used, this reduction is commonly described by a first-order model, and the kinetics can be described by the following equation:

$$\ln\left(A_t/A_0\right) = \ln\left(C_t/C_0\right) = -kt \quad (1)$$

where A_t and C_t represent the absorbance and concentration of the 4-NiP at the reaction time t, A_0 and C_0 are the absorbance and concentration values of the initial 4-NiP solution, and t is the residence time.[29]

The porous structure and hydrophilic character of this composite sponge are favorable to the adsorption of 4-NiP and the

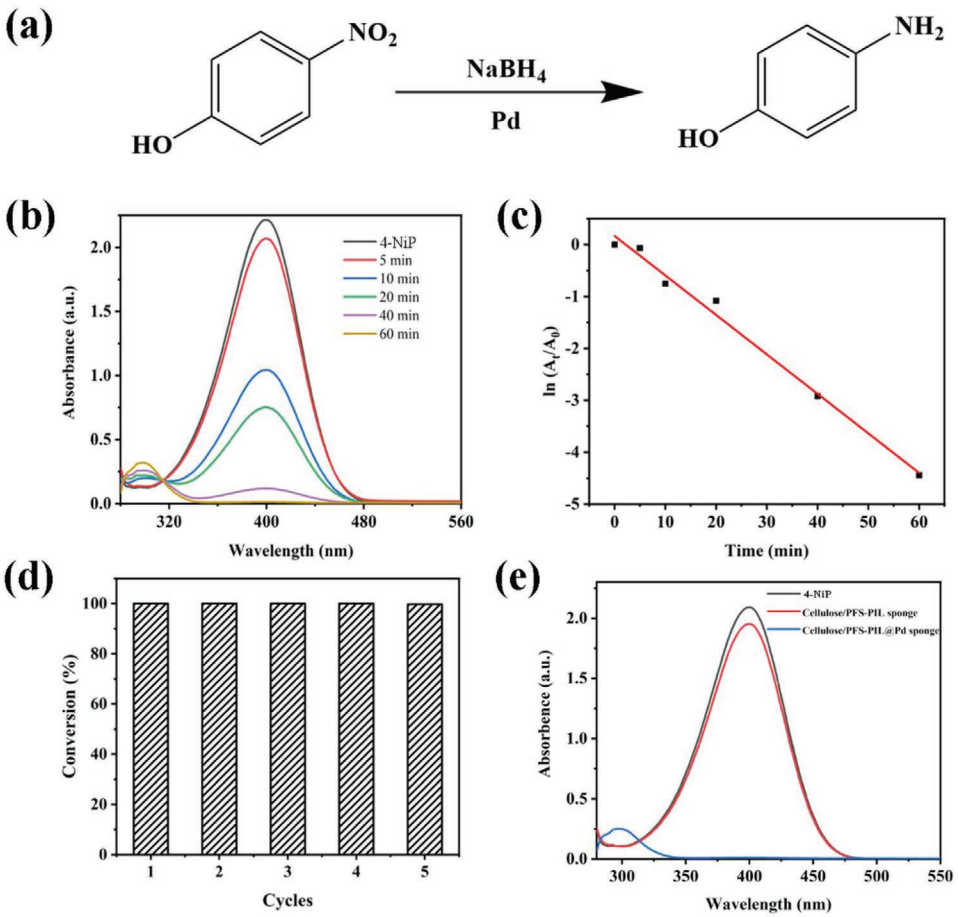

Figure 6. Catalysis with cellulose/PFS sponges. a) The chemical reaction of 4-NiP reduction to 4-aminophenol. b) Time-dependent UV–vis absorption spectra for the reduction of 4-NiP. c) Plots of ln (A_t/A_0) against reaction time for the catalytic reduction of 4-NiP. d) Cyclic reduction experiment of 4-NiP by one cellulose/PFS-PIL@Pd sponge. e) UV–vis absorption spectra for the reduction of 4-NiP with cellulose/PFS-PIL@Pd sponge and cellulose/PFS-PIL sponge.

transfer of 4-AmP. The Pd NPs are deposited into the sponge sheets and dispersed in the pores of the sponge material network, maximizing the number of active sites that can participate in the reduction.

Figure 6b shows the UV–vis absorption spectra. It took 60 min for cellulose/PFS-PIL@Pd sponge to complete the reduction of 4-NiP to 4-AmP. The reaction mixture changed from yellow to colorless (Figure S4, Supporting Information). Corresponding formation of 4-AmP was confirmed by GC-MS (Figure S5, Supporting Information). The relationship between ln (A_t/A_0) and the reaction time is shown in Figure 6c. After performing a linear fit, the value of the slope is -0.076 min^{-1}, yielding a rate constant value of $k = 0.076$ min^{-1}.

In addition, the same sponge was used for the reusability experiments. The cellulose/PFS-PIL@Pd sponge could be easily recovered from the solution by tweezers. The Pd NPs interact with the sponge sheets and are fixed in the sponge network, which made this NP loaded sponge very stable under the employed stirring condition. As displayed in Figure 6d, the sponge could be reused for at least five successive reaction cycles without loss of activity. This confirmed that the cellulose/PFS-PIL@Pd sponge possessed good reusability. The prolonged reaction time for the repeat experiments can be ascribed to the aggregation of NPs during the reuse process.[30]

The cellulose/PFS-PIL sponge without NPs was also used to catalyze the reaction. The results obtained are shown in Figure 6e. It is evident that no reaction occurred within the sponge without NPs. The slight decrease in the peak may be due to adsorption of reactants by the sponge.

2.7. Catalytic Performance of Cellulose/PFS-PIL@Pd2 Sponge

We now turn our attention to describing the catalytic performance of the second sponge type, which was freeze-dried prior to reduction of Pd NPs.

The cellulose/PFS-PIL@Pd sponges prepared by in situ reducing K_2PdCl_4 to Pd NPs, followed by freeze-drying, show a good performance in terms of catalytic activity and cycle stability. However, aggregation of metal NPs during the freeze-drying process and partial covering of metal NPs by the gel layer may limit their catalytic performance to a certain extent. In order to enhance the catalytic performance of cellulose/PFS-PIL@Pd sponges, the protocol for preparing these structures

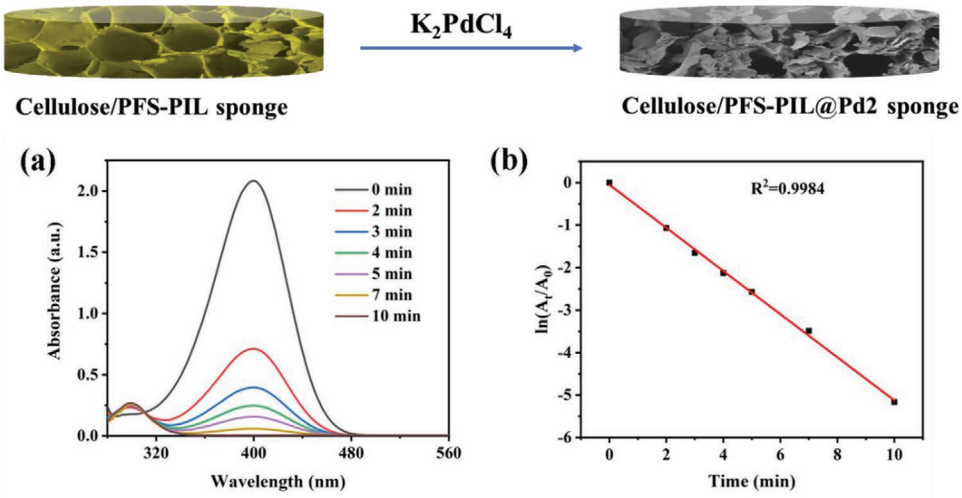

Figure 7. The efficiency of the catalytic cellulose/PFS-PIL@Pd2 sponge. a) Time-dependent UV–vis absorption spectra for the reduction of 4-NiP. b) Plots of ln (A_t/A_0) against reaction time for the catalytic reduction of 4-NiP.

was modified by changing the order of metal loading and freeze-drying. In the adapted approach, cellulose/PFS-PIL hydrogel was first freeze-dried to obtain a cellulose/PFS-PIL dry sponge, followed by in-situ reduction of K_2PdCl_4 to Pd NPs (cellulose/PFS-PIL@Pd2 sponge). Using this approach, it was expected that more NPs are present at the surface of the sponge walls and that aggregation, which might occur during the freeze-drying process, is prevented. The formation of Pd NPs in the cellulose/PFS-PIL@Pd2 sponge was confirmed by TEM, XPS, and TGA measurements (Figure S6, Supporting Information). The diameter of Pd NPs in cellulose/PFS-PIL@Pd2 sponge was mainly in the range of 3–6 nm (Figure S3d, Supporting Information).

Figure 7a records the UV–vis absorption spectra of the reduction of 4-NiP to 4-AmP using a cellulose/PFS-PIL@Pd2 sponge. Only 10 min were required to complete the redox process, which corresponds to a considerable rate enhancement of the reaction. Figure 7b shows the observed relationship between ln (A_t/A_0) and the reaction time. After performing a linear fit, the value of the slope shown is –0.51 min^{-1}, yielding a rate constant value of k = 0.51 min^{-1}. The catalytic activity of cellulose/PFS-PIL@Pd2 sponges in the reduction of 4-NiP to 4-AmP compares favorably with the activity of a variety of metal NPs in this reaction (**Table 1**). Pd NPs reduced by PFS-PIL without other external small molecular reducing agents can reach the same or better catalytic performance in the reduction of 4-NiP.

3. Conclusions

Palladium nanoparticle-loaded cellulose/PFS-PIL composite sponges were fabricated by codissolving cellulose and PFS-PIL, followed by solvent exchange and subsequent freeze-drying. PFS-PIL, possessing butylimidazolium side groups, could be uniformly mixed with cellulose in an ionic liquid. PFS-PIL reduced and immobilized metal NPs in an in situ process which required no external reducing agents. The porous cellulose/PFS-PIL sponges were found to be effective supports for Pd NPs. These sponges demonstrated excellent catalytic properties which could be further improved to reach a rate constant value of k = 0.51 min^{-1} for the reduction of 4-NiP to 4-AmP by a conscientious choice of the NP loading process. The method used to form and immobilize metal NPs on renewable support materials can be applied to create a broad range of metal NP-decorated porous structures.

Table 1. Rate constants k of 4-NiP reduction reactions catalyzed by various metal NPs.

Materials	k value [min^{-1}]	External reducing agents for metal NPs reduction	Refs.
Cellulosic protic ionic liquids hydrogel with Pd NPs	0.139	$NaBH_4$	[31]
Pd/Fe_3O_4/polypyrrole hollow capsules	0.122	$NaBH_4$	[32]
Chitosan/Pd nanocomposites	0.24	$NaBH_4$	[33]
Au NPs on chitosan-coated iron oxide magnetic nanocarrier	0.072	$NaBH_4$	[34]
Cu NPs embedded bacterial cellulose aerogels	0.56	$NaBH_4$	[9]
Cu and Ag NPs @ cellulose acetate nanocomposite	0.34	$NaBH_4$	[35]
Cellulose films decorated with gold NPs	0.40	Sodium citrate	[36]
Silver NPs/polydopamine coated polyvinyl alcohol sponge	0.072	$NaBH_4$	[37]
Pd NPs loaded cellulose–PFS hybrid sponges	0.51	/	This work

4. Experimental Section

Materials: Poly(ferrocenyl(3-iodopropyl)methylsilane) (PFS-I) (M_n: 2.93×10^5 g mol^{-1}, M_w: 1.27×10^5 g mol^{-1}) was prepared according to an established procedure.[38] Cellulose powder (ultrafine Arbocel UFC-100, JRS GmbH, Rosenberg, Germany), 1-butyl-3-methylimidazolium chloride (ionic liquid, TCI Europe, >98.0%), 1-butylimidazole (Aldrich, 98%), dimethylsulfoxide (DMSO, Biosolve), tetrahydrofuran (THF, Biosolve), sodium chloride (NaCl) (Aldrich, 99.5%), bis(trifluoromethane) sulfonimide lithium salt ($LiTf_2N$, Aldrich), dimethylformamide (DMF, Biosolve), potassium tetrachloropalladate(II) (K_2PdCl_4, Strem chemicals, 99%), 4-NiP (Fluka, ≥99.5%), sodium borohydride (Aldrich, 99%) were used without further purification. Water was purified with a Millipore system.

Characterization Methods: Molar mass values were determined by gel permeation chromatography in THF using a calibration curve based on narrow polystyrene standards. ^{1}H NMR spectra were recorded by employing a Bruker Avance III 400 MHz spectrometer and using DMSO-$_{d6}$ as the solvent. FTIR spectra were obtained by an Alpha spectrometer (Bruker). Morphologies of different sponges and Pd NPs were recorded by SEM (JSM-7610FPlus, JEOL) and TEM (CM300, FEI/Philips). XPS was recorded on a PHI Quantera SXM-XPS system. A monochromatic Al Kα radiation source at 1486.6 eV was used with a 100 µm diameter beam and 25 W X-ray gun power. The base pressure of the chamber was 5.4×10^{-10} Torr, and the working pressure was 3.0×10^{-8} Torr (argon). The beam input and detector input angles were 45°. TGA (TGA550, TA Instruments) was used to characterize the relative compositions of three different kinds of sponges. TGA was performed in an N_2 atmosphere from 30 to 600 °C at a rate of 20 °C min^{-1}. ICP was used to quantify the Pd content (Prodigy-ICP, Leeman). The concentration of reactants in the aqueous solutions were monitored using UV-Vis (LAMBDA 850, Perkin Elmer).

Synthesis of PFS-Butylimidazolium Tf2N (PFS-PIL): PFS-butylimidazolium Tf_2N (PFS-C_4IM Tf_2N, PFS-PIL) was synthesized according to a previously published procedure.[39] 1-Butylimidazole (0.37 g, 3.0 mmol) and DMSO (6 mL) were added to a solution of PFS-I (0.4 g, 1.0 mmol) in THF (12 mL). The mixture was stirred at 60 °C for 24 h. After removing THF, the mixture was transferred into a Spectra/Por 4 dialysis hose (MWCO 12–14 000 g mol^{-1}) and dialyzed against 0.1 M NaCl (3 × 8 L) and MilliQ water (3 × 8 L). Concentration of salt-free polyelectrolyte solution by a flow of N_2 produced PFS-C_4IM chloride as orange flakes. The ^{1}H NMR spectrum of PFS-C_4IM chloride is shown in Figure S1 (Supporting Information). Yield: 0.39 g, 89%. PFS-C_4IM Tf_2N was prepared by subsequent counterion exchange with Tf_2N^- ions. PFS-C_4IM chloride solution was dropwise added to an aqueous $LiTf_2N$ solution (the molar ratio of PFS-C_4IM chloride and $LiTf_2N$ was 1:3). The resulting precipitate was washed with deionized water three times. PFS-C_4IM Tf_2N was obtained as an orange powder. Yield: 0.52 g, 86%.

Preparation of Cellulose/PFS-PIL@Pd Sponge: First, the cellulose powder was added to ionic liquid (4 wt%) and heated to 95 °C for 2 h to reach dissolution. Meanwhile, PFS-PIL was dissolved in DMF (1 mg mL^{-1}). The PFS-PIL solution was then added to the cellulose/ionic liquid solution at a given PFS-PIL:cellulose weight ratio of 1:4, which resulted in a uniform orange solution. The mixed solution was poured into a small beaker and placed in a vacuum oven at 85 °C for 4 h to remove DMF to obtain a transparent and viscous solution. After cooling, the viscous solution acquired an ionogel state.

The ionogel was placed in deionized water for solvent exchange, and an orange hydrogel was obtained. Then, the hydrogel was placed in a solution containing 0.1×10^{-3} M K_2PdCl_4. The PFS chains of the hydrogel reduced this salt to Pd NPs, and the color of the hydrogel became dark brown. Finally, the dark brown hydrogel was placed in a freezer (−28 °C) and subsequently dried by freeze drying over 48 h to obtain a dark brown sponge referred to as cellulose/PFS-PIL@Pd sponge. The orange cellulose/PFS-PIL hydrogel was also frozen at −28 °C and dried in a freeze dryer for 48 h to obtain an orange sponge referred to as cellulose/PFS-PIL sponge. The colorless cellulose hydrogel was subjected to the same steps, which yielded a white sponge referred to as cellulose sponge.

Preparation of Cellulose/PFS-PIL@Pd2 Sponge: Immersion of freeze-dried cellulose/PFS-PIL sponge in 1×10^{-3} M K_2PdCl_4 solution led to the in situ formation and immobilization of Pd nanoparticles in the porous structure, yielding cellulose/PFS-PIL@Pd2 sponges. During this process, the porous structure of the sponge remained intact. After completion of the metal loading step, the sponge was washed three times with deionized water.

Catalytic Performance of Cellulose/PFS-PIL@Pd Sponge: The catalytic performance was evaluated by the reduction of 4-NiP to 4-AmP. First, 250 µL of 4-NiP solution (0.01 M) was added to 25 mL of $NaBH_4$ solution (0.4 mg mL^{-1}) under stirring. Afterwards, a piece of the cellulose/PFS-PIL@Pd sponge (around 10 mg, first wetted by deionized water) was put into the solution. The remaining concentration of 4-NiP (λ_{max} = 400 nm) was determined by UV–Vis absorption spectroscopy at a given time. Finally, the sponges were recovered from the reaction by tweezers, rinsed with deionized water, and then reused in the next cycle.

Supporting Information

Supporting Information is available from the Wiley Online Library or from the author.

Acknowledgements

The authors thank the MESA+ Institute of Nanotechnology of the University of Twente for financial support. H.C. appreciates the Chinese Scholarship Council for providing a scholarship. The authors acknowledge Mr. Clemens Padberg for the SEM imaging and Mr. Giorgos Kafkopoulos for the TGA analysis.

Conflict of Interest

The authors declare no conflict of interest.

Data Availability Statement

The data that support the findings of this study are available from the corresponding author upon reasonable request.

Keywords

catalysis, cellulose, palladium nanoparticles, poly(ferrocenylsilane), polyionic liquid

Received: September 1, 2021
Revised: November 25, 2021
Published online:

[1] a) L. He, F. Weniger, H. Neumann, M. Beller, *Angew. Chem., Int. Ed.* **2016**, *55*, 12582; b) D. Astruc, F. Lu, J. R. Aranzaes, *Angew. Chem., Int. Ed.* **2005**, *44*, 7852.

[2] a) X. Pei, Y. Deng, B. Duan, T.-S. Chan, J.-F. Lee, A. Lei, L. Zhang, *Nano Res.* **2018**, *11*, 3145; b) T. Hees, F. Zhong, T. Rudolph, A. Walther, R. Mülhaupt, *Adv. Funct. Mater.* **2017**, *27*, 1605586.

[3] P. Xu, C. Cen, N. Chen, H. Lin, Q. Wang, N. Xu, J. Tang, Z. Teng, *J. Colloid Interface Sci.* **2018**, *526*, 194.

[4] a) Z. Xiang, Y. Chen, Q. Liu, F. Lu, *Green Chem.* **2018**, *20*, 1085; b) X. Yang, H. Zhong, Y. Zhu, H. Jiang, J. Shen, J. Huang, C. Li, *J. Mater. Chem. A* **2014**, *2*, 9040.

[5] a) Q. Yang, Q. Xu, H.-L. Jiang, *Chem. Soc. Rev.* **2017**, *46*, 4774; b) Y. Liu, K. Zhang, W. Li, J. Ma, G. J. Vancso, *J. Mater. Chem. A* **2018**, *6*, 7741.
[6] a) J. Gu, C. Hu, W. Zhang, A. B. Dichiara, *Appl. Catal., B* **2018**, *237*, 482; b) R. J. White, R. Luque, V. L. Budarin, J. H. Clark, D. J. Macquarrie, *Chem. Soc. Rev.* **2009**, *38*, 481.
[7] a) D. Klemm, F. Kramer, S. Moritz, T. Lindström, M. Ankerfors, D. Gray, A. Dorris, *Angew. Chem., Int. Ed.* **2011**, *50*, 5438; b) D. Klemm, E. D. Cranston, D. Fischer, M. Gama, S. A. Kedzior, D. Kralisch, F. Kramer, T. Kondo, T. Lindström, S. Nietzsche, *Mater. Today* **2018**, *21*, 720.
[8] a) Y. Li, L. Xu, B. Xu, Z. Mao, H. Xu, Y. Zhong, L. Zhang, B. Wang, X. Sui, *ACS Appl. Mater. Interfaces* **2017**, *9*, 17155; b) Q. Zhang, L. Zhang, W. Wu, H. Xiao, *Carbohydr. Polym.* **2020**, *229*, 115454; c) C. Zhang, M. Zhou, S. Liu, B. Wang, Z. Mao, H. Xu, Y. Zhong, L. Zhang, B. Xu, X. Sui, *Carbohydr. Polym.* **2018**, *191*, 17; d) H. Cheng, L. Li, B. Wang, X. Feng, Z. Mao, G. J. Vancso, X. Sui, *Prog. Polym. Sci.* **2020**, *106*, 101253.
[9] L. Song, L. Shu, Y. Wang, X.-F. Zhang, Z. Wang, Y. Feng, J. Yao, *Int. J. Biol. Macromol.* **2020**, *143*, 922.
[10] S. Keshipour, M. Khezerloo, *J. Iran. Chem. Soc.* **2017**, *14*, 1107.
[11] H. Duan, D. Wang, Y. Li, *Chem. Soc. Rev.* **2015**, *44*, 5778.
[12] M. Kaushik, A. Moores, *Green Chem.* **2016**, *18*, 622.
[13] R. L. Hailes, A. M. Oliver, J. Gwyther, G. R. Whittell, I. Manners, *Chem. Soc. Rev.* **2016**, *45*, 5358.
[14] a) K. Zhang, X. Feng, C. Ye, M. A. Hempenius, G. J. Vancso, *J. Am. Chem. Soc.* **2017**, *139*, 10029; b) K. Zhang, M. Zhang, X. Feng, M. A. Hempenius, G. J. Vancso, *Adv. Funct. Mater.* **2017**, *27*, 1702784.
[15] K. Zhang, X. Feng, X. Sui, M. A. Hempenius, G. J. Vancso, *Angew. Chem., Int. Ed.* **2014**, *53*, 13789.
[16] X. Feng, M. A. Hempenius, G. J. Vancso, *Macromol. Chem. Phys.* **2018**, *219*, 1800223.
[17] X. Sui, X. Feng, M. A. Hempenius, G. J. Vancso, *J. Mater. Chem. B* **2013**, *1*, 1658.
[18] Q. Zhao, P. Zhang, M. Antonietti, J. Yuan, *J. Am. Chem. Soc.* **2012**, *134*, 11852.
[19] a) D. M. Phillips, L. F. Drummy, D. G. Conrady, D. M. Fox, R. R. Naik, M. O. Stone, P. C. Trulove, H. C. De Long, R. A. Mantz, *J. Am. Chem. Soc.* **2004**, *126*, 14350; b) H. Zhang, J. Wu, J. Zhang, J. He, *Macromolecules* **2005**, *38*, 8272.
[20] a) J. Zhang, H. Zhang, J. Wu, J. Zhang, J. He, J. Xiang, *Phys. Chem. Chem. Phys.* **2010**, *12*, 1941; b) J. Zhang, J. Wu, J. Yu, X. Zhang, J. He, J. Zhang, *Mater. Chem. Front.* **2017**, *1*, 1273.
[21] Y. Si, X. Wang, C. Yan, L. Yang, J. Yu, B. Ding, *Adv. Mater.* **2016**, *28*, 9512.
[22] a) P. Zhang, Y. Gong, H. Li, Z. Chen, Y. Wang, *Nat. Commun.* **2013**, *4*, 1593; b) T. Teranishi, M. Miyake, *Chem. Mater.* **1998**, *10*, 594.
[23] Z. Dai, J. Bradley, D. Joswiak, D. Brownlee, H. Hill, M. Genge, *Nature* **2002**, *418*, 157.
[24] S. Yang, J. Dong, Z. Yao, C. Shen, X. Shi, Y. Tian, S. Lin, X. Zhang, *Sci. Rep.* **2014**, *4*, 4501.
[25] R. Petersen, D. A. Foucher, B.-Z. Tang, A. Lough, N. P. Raju, J. E. Greedan, I. Manners, *Chem. Mater.* **1995**, *7*, 2045.
[26] a) F. Costantini, E. M. Benetti, R. M. Tiggelaar, H. J. Gardeniers, D. N. Reinhoudt, J. Huskens, G. J. Vancso, W. Verboom, *Chem. - Eur. J.* **2010**, *16*, 12406; b) J. Strachan, C. Barnett, A. F. Masters, T. Maschmeyer, *ACS Catal.* **2020**, *10*, 5516.
[27] a) S. Wunder, Y. Lu, M. Albrecht, M. Ballauff, *ACS Catal.* **2011**, *1*, 908; b) S. Wunder, F. Polzer, Y. Lu, Y. Mei, M. Ballauff, *J. Phys. Chem. C* **2010**, *114*, 8814.
[28] W. Lu, R. Ning, X. Qin, Y. Zhang, G. Chang, S. Liu, Y. Luo, X. Sun, *J. Hazard. Mater.* **2011**, *197*, 320.
[29] H. Koga, E. Tokunaga, M. Hidaka, Y. Umemura, T. Saito, A. Isogai, T. Kitaoka, *Chem. Commun.* **2010**, *46*, 8567.
[30] J. Han, L. Li, R. Guo, *Macromolecules* **2010**, *43*, 10636.
[31] X. Li, F. Dong, L. Zhang, Q. Xu, X. Zhu, S. Liang, L. Hu, H. Xie, *Chem. Eng. J.* **2019**, *372*, 516.
[32] T. Yao, Q. Zuo, H. Wang, J. Wu, B. Xin, F. Cui, T. Cui, *J. Colloid Interface Sci.* **2015**, *450*, 366.
[33] S. Dhanavel, N. Manivannan, N. Mathivanan, V. K. Gupta, V. Narayanan, A. Stephen, *J. Mol. Liq.* **2018**, *257*, 32.
[34] Y.-C. Chang, D.-H. Chen, *J. Hazard. Mater.* **2009**, *165*, 664.
[35] F. U. Khan, S. B. Khan, T. Kamal, A. M. Asiri, I. U. Khan, K. Akhtar, *Int. J. Biol. Macromol.* **2017**, *102*, 868.
[36] C. R. Cabreira, F. F. Camilo, *Cellulose* **2020**, *27*, 3919.
[37] M. Guo, Y. Zhang, F. Du, Y. Wu, Q. Zhang, C. Jiang, *Mater. Chem. Phys.* **2019**, *225*, 42.
[38] M. A. Hempenius, F. F. Brito, G. J. Vancso, *Macromolecules* **2003**, *36*, 6683.
[39] X. Sui, M. A. Hempenius, G. J. Vancso, *J. Am. Chem. Soc.* **2012**, *134*, 4023.